Oxidation of sputter-deposited vanadium nitride as a new precursor to achieve thermochromic VO 2 thin films

A.C. C García-Wong, D. Pilloud, S. Bruyère, S. Mathieu, S. Migot, J.F. Pierson, F. Capon

Oxidation of sputter-deposited vanadium nitride as a new precursor to achieve thermochromic VO_2 thin films

A.C. García-Wong[a], D. Pilloud[a], S. Bruyère[a], S. Mathieu[a], S. Migot[a], J.F. Pierson [a,*], F. Capon[a]

[a] Institut Jean Lamour (UMR CNRS 7198), Université de Lorraine, 54000 Nancy, France

* Corresponding author e-mail: jean-francois.pierson@univ-lorraine.fr

Abstract

Elaboration of VO_2 films with good thermochromic properties remains a challenge because it is mandatory to avoid other intermediate phases belonging to the vanadium-oxygen system. In this work, we propose vanadium nitride (VN) as a new precursor to obtain thermochromic VO_2. VN films were reactively sputter-deposited on Si substrates by using an in-line semi-industrial machine. The films of 175 nm thickness were submitted to an annealing process implemented at different durations at 450°C. X-ray diffraction and Raman spectrometry were performed for structural characterizations of the oxidized films showing the presence of monoclinic VO_2 in a wide range of oxidation time. As the annealing time increased, V_2O_5 appeared to affect the performance of the oxidized films. The TEM analysis carried out on the oxidized sample for 25 minutes showed that there is an abrupt interface between VN and VO_2. The thermal-induced properties of the studied films were analyzed in terms of their electrical resistance employing a

four-point probe method and their emissivity modulation properties by infrared camera. The results showed a thermochromic behavior for the samples oxidized in the range of 15-35 min. On the contrary, the presence of residual VN layers in samples oxidized for less than 15 min and V_2O_5 in the ones annealed for more than 35 min hindered the thermochromic behavior of these films. Bringing together all the characterization techniques used a phase diagram of VN oxidation was plotted. The results of this work suggest that VN is an interesting new precursor to synthesize thermochromic VO_2 films.

Keywords: Vanadium dioxide; Vanadium Nitride; Thermochromism; Optical and electrical properties

1. Introduction

In 1959, Morin demonstrated that vanadium dioxide (VO_2) exhibits a reversible metal-insulator transition (MIT) approximately at T_c = 68°C [1]. At low temperature, VO_2 behaves as a semiconductor with a monoclinic structure, high transmittance in the infrared region and high electrical resistivity, while at temperatures higher than T_c a transition to a metallic tetragonal rutile structure occurs and VO_2 exhibits low transmittance and low electrical resistivity. The change of these properties during the phase transition of VO_2 makes this material convenient for several applications, such as infrared modulation in smart windows [2–8], thermal solar collectors [9,10], dynamic thermal control of spacecraft [11–13], ultrafast electronic devices [14,15] and many others. Although the research on this material has been carried on for several decades, the synthesis of VO_2 films with good thermochromic properties on large surfaces still remains a challenge. The reason behind this defiance is the imperative need to avoid several other phases in the vanadium-oxygen system [16].

Magnetron sputtering is one of the most used methods to produced VO_2. Among the different approaches to obtain VO_2, reactive sputtering in a mixture of Ar and O_2 without a post-annealing process is one of the most used [11,17–21]. However, the need to properly control the O_2 flow rate makes this method not suitable on large surfaces. On the other hand, a post-annealing process in air or oxygen is commonly used to improve the quality of the deposited films [22–25]. Another interesting and simple proposal is the Sputtering Oxidation Coupling (SOC) method. It is a two-stage procedure, in which a vanadium film is deposited and then annealed in a furnace outside of the deposition chamber [26]. The possibility to regulate the temperature and duration during the oxidation process makes this method suitable and attractive for the industrial process.

In this study, we chose to modify the SOC method using another precursor: vanadium nitride (VN). At room temperature, the NaCl-like structure of the VN phase is more resistant to oxidation than the body-cubic centered of the V one [27,28]. Besides, several studies have shown that the oxidation of VN at elevated temperatures resulted in the formation of a series of vanadium oxides, which significantly improved the tribological properties of the film [29,30]. Nevertheless, to the best of our knowledge, controlled oxidation of VN has never been performed to produce thermochromic VO_2.

In this paper, VN thin films are reactively sputter-deposited on Si substrates. The air-oxidation conditions of these films have been optimized. The results indicate that VN is an interesting new precursor to synthesize high-quality thermochromic VO_2 films.

2. Experimental details

VN thin films were deposited on undoped (100) silicon substrates by reactive magnetron sputtering of a metallic vanadium target (330 mm length, 50 mm width, 6 mm thick and 99.95% purity) in an Ar-N_2 mixture with flow rates of 30 and 5 standard cubic centimeters per minute (sccm), respectively. The deposition pressure was fixed to 1 Pa and no intentional heating was used during growth. A pulsed-DC power supply (Pinnacle + Advanced Energy), working on a set current of 1.5 A, provided power to the V target. The frequency of DC-pulses and their off-time were kept at 50 kHz and 4 μs, respectively. The distance between target and substrate was 5 cm. The volume of the semi-industrial chamber is around 350 L. The Si wafer (4 inches diameter) fixed to the substrate holder moved back and forth in front of the V target (to ensure films homogeneity) at a speed of 50 cm/min during 1 h. The 175 nm thickness of the VN film was measured by a GBS Smart WLI 3D optical profilometer.

The second step consisted of air-oxidation of the VN films to form vanadium oxide films. The as-deposited VN films were annealed in a modified Carbolite HRF 7/45 furnace equipped with a quick sample tray loader to prevent any drop in the temperature when the sample is introduced. The furnace worked under atmospheric pressure at a preheated temperature of 450°C during different durations 7, 10, 15, 20, 25, 30, 35, 40 and 50 minutes. The films were labeled “VN” for as-deposited vanadium nitride films and “VN_time” for the oxidized films for various annealing durations.

X-rays diffractograms (XRD) were collected by using a Bruker D8 Advanced diffractometer with Cu $K_{\alpha 1}$ radiation (λ = 1.5406 Å) in the Bragg−Brentano configuration. Raman spectra of samples were acquired on a Horiba Jobin-Yvon LabRAM spectrometer. Samples were excited by a Nd:YAG laser (532 nm) with a power of approximately 10 mW. This laser beam power was low enough to avoid any heating effect (such as oxidation from VO_2 to V_2O_5). The morphology of the films was studied by scanning electron microscopy (SEM) in a ZEISS GeminiSEM 500. All images were taken by using an Inlens secondary electron detector and under the same conditions: magnification of x100000 and a low acceleration voltage of 1 kV. Transmission electron microscopy (TEM) was carried out in the sample oxidized for 25 minutes with a JEOL ARM 200-Cold FEG (point resolution 0.19 nm). The cross-section TEM sample was prepared by a focused ion beam (FIB)-SEM dual beam system (FEI Helios Nanolab 600i). Electron energy loss spectroscopy (EELS) experiments were carried out in scanning electron transmission microscopy mode (STEM). The spectrometer was set to an energy dispersion of 0.1 eV/channel and the resolution of the full width at half maximum (FWHM) of the zero-loss peak was 0.7 eV.

The study of the sheet resistance as a function of the temperature of the samples was performed by the four-point probe method (Jandel) equipped with a Linkam® HFS600E heater system in the 30-120°C temperature range.

The dependence of optical properties of the films with temperature (30-120°C range) was investigated by using an infrared camera (FLIR A300) that supplies a cumulative response sensitive in the 7.5-13 μm spectral range. The emissivity of the oxidized VN films was calculated from the slope of the temperature measured using the IR camera (T_{IR}) as a function of the real temperature (T_S) of the sample. Measurements were carried out by considering $\varepsilon = 1$ irrespective to the sample. Besides, T_S was measured using a Prazitherm heater system. The emissivity switch, $\Delta\varepsilon = \varepsilon_{HT} - \varepsilon_{LT}$ (ε_{HT} corresponds to the emissivity at high temperature and ε_{LT} corresponds to the emissivity at low temperature) was determined by the difference between the slopes corresponding to each region of the MIT according to the procedure employed by Benkahoul et al [11].

3 Results

3.1 Microstructure and morphology

The X-ray diffractograms for as-deposited and air annealed VN films deposited on silicon are shown in Fig. 1. VN films (175 nm thick) exhibit two peaks located at approx. 37.9° and 80.3° corresponding to (111) and (222) planes of the face-centered cubic VN structure (PDF no.00-035-0768), respectively. No other peak is detected except those of silicon substrate. Fig. 1 also presents diffractograms for the films after air-annealing at 450°C during different durations in the 7-50 min range. For the lowest duration, the monoclinic VO_2 phase is not detected. However, the intensity of the VN peaks diminishes, which indicates that the oxidation process has effectively begun. In

addition, these peaks are shifted to higher angles because of stress relaxation during the oxidation process. As the annealing time increases, the VN peaks intensity decreases even more and the main (111) peak is noticed up to 25 min, indicating the presence of a remaining layer of vanadium nitride. Monoclinic VO_2 is detected for the first time after 10 min of air oxidation. The most significant peaks corresponding to m-VO_2 are located at 2θ = 37.1, 42.3 and 72.1° (PDF no. 04-003-2035), showing that the oxide layer corresponds to an equiaxed structure (i.e. that it does not grow with a strong preferred orientation). The most intense peak of VO_2 appears at 30 min of oxidation and the VN peak completely disappears at the same time. In this sample (VN_30), two new peaks with a low intensity corresponding to orthorhombic V_2O_5 phase are detected (PDF no. 00-041-1426). For oxidation times greater than 30 min, the peaks corresponding to VO_2 decrease in intensity while the opposite occurs with the peaks of V_2O_5. For the VN_50 sample, the VO_2 vanishes, leading to the V_2O_5 being the only crystalline phase present. These results show oxidation from V^{4+} state to V^{5+} state as the oxidation time increases and are consistent with the findings of several authors [24,31].

Due to the overlapping of the diffraction peaks of the various vanadium oxide phases, X-ray diffraction is not a powerful method to evince the formation of a pure VO_2 phase. To verify the formation of VO_2, cross-examination with Raman spectrometry is carried out for all oxidized films. Figure 2 presents room-temperature Raman spectra of the oxidized VN films, deposited on silicon substrates.

The Si substrate signal (520 cm^{-1}) is barely visible until 10 min of oxidation, thanks to the presence of the VN film that exhibits metallic behavior. As the oxidation time increases the Si signal becomes more perceptible indicating a decrease of the VN layer thickness. From sample

VN_25, the peak at 520 cm^{-1} is intense; suggesting that the sample is almost completely oxidized, as shown by XRD. Thus, the evolution of the Si Raman band is a powerful tool to monitor the VN oxidation.

Oxidized samples in the range of 10 to 25 min show relatively similar vibration bands, with most of the peaks (located at approx. 192, 223, 264, 296, 331, 389, 499 and 622 cm^{-1}) assigned to m-VO_2 phase, in accordance with literature data [32–35].

In the case of the oxidized films during 40 and 50 minutes, the shape of the spectra is different from the other samples. The vibration bands detected at approx. 195, 284, 303, 405, 528, 701 and 992 are readily assigned to the V_2O_5 phase [32,36].

The simultaneous presence of VO_2 and V_2O_5 is detected by X-ray diffraction results in oxidized samples between 30 and 40 min. Although several bands may overlap, it is difficult to notice a big change in the spectrum of these samples. However, one can notice a slight shift of the band located at 389 cm^{-1} (VN_20 sample) until reaching 405 cm^{-1} (VN_40 sample). The Raman results confirm the formation of VO_2 and V_2O_5 as shown by the X-ray results.

Fig. 3 shows the top view SEM images of six relevant samples: the as-deposited VN films and samples oxidized during 10, 20, 25, 30 and 50 min, respectively. The VN film exhibits a surface morphology with small triangular grains in agreement with the [111] preferred orientation observed by XRD. Throughout the oxidation process, a drastic change in the morphology of the samples is noticed when compared to as-deposited VN films. After 10 minutes of oxidation (Fig. 3 b)), the surface changes and the triangular grains of VN are not perceived anymore. The oxidized VN grains coalesce into an elongated structure, increasing grain size. As oxidation continued, the

morphology of the samples does not change significantly and the grain size continues to grow. In all the images, the grain boundaries are clear and well defined.

Fig. 4 a) shows transmission electron microscopy micrograph for the VN_25 sample. The figure displayed that there is no well-defined shape for the "supposed" VO_2 grains (two regions with different morphologies) and there is still residual VN, as observed in XRD. Moreover, the presence of vanadium nitride is not continuous on the surface of the sample. To check the presence of VO_2 in the sample, a high-resolution TEM (HRTEM) micrograph with the corresponding fast Fourier transform pattern (FFT) investigation is conducted in the area enclosed in red in Fig. 4 a) (Fig. 4 b) and Fig. 4 c), respectively). It was possible to identify the (111), (010) and (101) planes of VO_2. The obtained interplanar distances are 0.229, 0.452 and 0.484 nm for the (111), (010) and (101) planes, respectively, in agreement with those reported for monoclinic VO_2 (PDF no. 04-003-2035).

From Fig. 4 one cannot discern whether areas with different colors and shapes belong to the same compound. To better elucidate this, an EELS characterization is performed in a region of the sample where VN and VO_2 coexist (Fig. 5 a)). The high angle annular dark field image shows different morphologies and colors. VN with a columnar structure is evidenced close to the substrate. The region adjacent to the VN presents a light gray color and an almost rectangular shape; it was already proved that corresponds to VO_2. On the other hand, the region close to the film surface has a dark grey color and contains elongated grains. These grains present two pronounced differences concerning the morphology of the VN: they are thicker and are not perpendicular to the substrate, indicating that during the oxidation process a coalescence of the oxide grains occurs.

EELS spectra are recorded in four zones (labeled from 1 to 4) of Fig. 5 a), the results are shown in Fig. 5 b). In zone 1 there are only peaks corresponding to V (V_{L3} = 513 eV and V_{L2}= 521 eV) and N (N_K = 401 eV), confirming the presence of a remaining vanadium nitride layer. It is important to notice that region 3 is at the interface between the areas with different shapes and intensities of gray. In zones 2, 3 and 4 the spectra are very similar. Only peaks belonging to V (the same peaks of zone 1) and O (O_K = 532 eV) are evidenced, indicating that nitrogen is not present in this area anymore. Since the ratio of the V/O peaks intensity and as well as the peak position are constant, the zones labeled 2, 3 and 4 seem to contain the same oxide phase that corresponds to VO_2.

3.2 Optical and electrical properties

Near the MIT transition of VO_2, some physical properties present a hysteresis between the heating and cooling cycles. Within these properties, changes in electrical resistivity and emissivity at low and high temperatures are considered as indicators of VO_2 quality [25,37,38]. The higher the difference, the better the thermochromic properties.

For all oxidized samples, the optical modulation properties in the infrared (IR) domain are studied using an infrared camera. Fig. 6 represents apparent infrared temperature (T_{IR}) of samples monitored versus the sample temperature (T_S) during both, heating and cooling for the studied films. All the films of Fig. 6 exhibit hysteresis loops near the MIT region. Samples oxidized for 10 minutes or less show no representative thermochromic behavior ($\Delta\varepsilon_{VN_{10}} = -0.03$). This is due to the presence of a considerable residual layer of VN (see Fig. S1 in the supplementary information), higher oxidation time is needed to observe thermochromic behavior. A thermochromic effect is not observed for samples oxidized for a duration longer or equal to 40 min, $\Delta\varepsilon_{VN\_40} = -0.03$. In this

case, this is attributed to the increased formation of V_2O_5 phase with oxidation time. On the contrary, for samples oxidized in the range of 15 and 35 minutes, a thermochromic behavior with values of $\Delta\varepsilon$ between -0.14 and -0.20 is evidenced, confirming the presence of m-VO_2 consistent with XRD and Raman results. Nevertheless, the emissivity contrast obtains from our samples is lower than that reported in the literature. For example, Benkahoul et al. found $\Delta\varepsilon = -0.36$ in 300 nm thick VO_2 film deposited on Si [11]. Emissivity switching properties can be improved by modifying the temperature and duration of the air-annealing process (see Fig. S2 in the supplementary information), thickness changes [20,39] and doping [2,9,13].

Fig. 7 shows the evolution of the sheet resistance (SR) as a function of the temperature for all oxidized samples during both heating and cooling. In this study, sheet resistance is calculated rather than the resistivity, due to the presence of the remaining metallic VN layer for films oxidized for less than 25 minutes. Up and down triangles in Fig. 7 represent the profiles for temperature ramping up and down, respectively. The samples oxidized during 7 and 50 min do not evidence any hysteresis. For the low time oxidation duration (7 minutes) there is no remarkable change between low and high temperatures sheet resistance values, this is due to the presence of a remaining layer of VN. On the other hand, the sample oxidized for a long duration (50 minutes) displays no sign of VO_2, only V_2O_5. All other studied samples exhibit hysteresis loops in the near MIT region with different magnitudes: from a feeble smoothed hysteresis for VN_10, that rises to maximum marked hysteresis curves for VN_25 and then decreases again until an almost imperceptible hysteresis for VN_50. The enlarging presence of V_2O_5 in the samples oxidized for more than 25 minutes, is the reason for the reduction of the difference between the values of sheet resistance at low and high temperatures. These hysteresis loops are an intrinsic feature of thermochromic VO_2 MIT and, again confirm the XRD, Raman and IR thermometry results for the series of studied samples.

The thermochromic behavior of oxidized samples will be affected if they remain exposed to air open contact because the oxidation process continues. Infrared camera measurement of the oxidized sample 25 minutes was repeated 10 months later, showing a significant decrease (50%) in the absolute value of the emissivity switch (Fig. S3 supporting information). To protect the films for further and undesired oxidation anti-reflective layers such as TiO_2 [40,41], SiO_2 [42], AZO [43] and SiN_x [44] are used.

3.2 Phase diagram of VN oxidation at 450 °C

Gathering the results of XRD and Raman, as well as the study of optical and electrical properties, it is possible to obtain a phase diagram of VN oxidation.

In Fig. 8 is displayed on the left axis (blue squares) the logarithm of the ratio between the sheet resistance at low (SR_{LT}, measured at 30°C), and at high temperatures (SR_{HT}, measured at 120°C) as a function of the oxidation time for all the oxidized samples. The right axis (red circles) of the same figure shows the dependence of the emissivity switch with the oxidation time for all studied samples.

A color gradient is used in Fig. 8 to illustrate the five different regions that exist in the oxidation of VN at 450 °C. The first region is a VN predominant zone. As the oxidation time progresses, a region with the coexistence of VN and VO_2 appears. By increasing the annealing duration in this region, the ratio between SR_{LT} and SR_{HT} (the emissivity switch) increases (decreases) due to the competing effect of VO_2 formation with simultaneous VN degradation. During the interval between 25 and 30 min, there are the best thermochromic properties due to the almost complete oxidation of VN, where VO_2 is the predominant compound. Beyond 30 min, the amount of VO_2 declines and begins the formation of V_2O_5. Continuing with the oxidation process in this region, thermochromic performance decays as the amount of VO_2 diminishes while the presence of V_2O_5

rises. This reduction of thermochromic behavior is evident at 40 min of oxidation. Finally, as oxidation time continues to increase, there is a region where V_2O_5 is the only compound because of the over-oxidation of the samples.

4 Conclusions

This study reveals that VN is a new efficient precursor to achieve a high-quality monoclinic VO_2 using a sputtering oxidation coupling method. In correspondence with previous studies of oxidation of vanadium films, the importance of optimizing the annealing duration to obtain thermochromic vanadium dioxide is demonstrated. During the oxidation process at 450 °C, there are only two phases corresponding to the V-O system, VO_2 and V_2O_5. The first oxide formed is VO_2, it is present in several samples oxidized between 10 and 40 min. On the other hand, V_2O_5 is only detected after the total oxidation of VN. The best thermochromic behavior is accomplished in the oxidized samples in the range between 25-35 min. However, it is important to point out that in these samples two phases coexist:

1- VN and VO_2 in the sample VN_25,

2- VO_2 and V_2O_5 in samples VN_30 and VN_35.

In both cases, VN and V_2O_5 represent a small fraction compared to the VO_2 content. Therefore, we could expect to obtain a sample with only VO_2 in the range between 25-30 minutes of oxidation, which could present better thermochromic behavior.

The TEM analysis performed on the oxidized sample for 25 minutes show that there is an abrupt interface between VN and VO_2.

Resulting VO_2 films exhibit thermochromic properties that are suitable for applications of VO_2 as smart windows or as thermal controllers.

Acknowledgments

This work was supported by the French PIA project “Lorraine Université d’Excellence”, reference ANR-15-IDEX-04-LUE. The authors acknowledge the financial support of the Contrat de Plan Etat-Région MatDS. They are also grateful to the Centre de Competence Davm (cc-Davm) of the Institut Jean Lamour for the semi-industrial chamber provision.

References

[1] F.J. Morin, Oxides Which Show a Metal-to-Insulator Transition at the Neel Temperature, Phys. Rev. Lett. 3 (1959) 34–36. https://doi.org/10.1103/PhysRevLett.3.34.

[2] C. Ji, Z. Wu, X. Wu, J. Wang, J. Gou, Z. Huang, H. Zhou, W. Yao, Y. Jiang, Al-doped VO_2 films as smart window coatings: Reduced phase transition temperature and improved thermochromic performance, Sol. Energy Mater. Sol. Cells. 176 (2018) 174–180. https://doi.org/10.1016/j.solmat.2017.11.026.

[3] S.-Y. Li, G.A. Niklasson, C.G. Granqvist, Thermochromic undoped and Mg-doped VO_2 thin films and nanoparticles: Optical properties and performance limits for energy efficient windows, J. Appl. Phys. 115 (2014) 053513. https://doi.org/10.1063/1.4862930.

[4] X. Liang, M. Chen, Q. Wang, S. Guo, L. Zhang, H. Yang, Active and passive modulation of solar light transmittance in a hybrid thermochromic soft-matter system for energy-saving smart window applications, J. Mater. Chem. C. 6 (2018) 7054–7062. https://doi.org/10.1039/C8TC01274A.

[5] C. Ji, Z. Wu, L. Lu, X. Wu, J. Wang, X. Liu, H. Zhou, Z. Huang, J. Gou, Y. Jiang, High thermochromic performance of Fe/Mg co-doped VO_2 thin films for smart window applications, J. Mater. Chem. C. 6 (2018) 6502–6509. https://doi.org/10.1039/C8TC01111G.

[6] H. Ji, D. Liu, H. Cheng, C. Zhang, Inkjet printing of vanadium dioxide nanoparticles for smart windows, J. Mater. Chem. C. 6 (2018) 2424–2429. https://doi.org/10.1039/C8TC00286J.

[7] Y. Kim, S. Yu, J. Park, D. Yoon, A.M. Dayaghi, K.J. Kim, J.S. Ahn, J. Son, High-throughput roll-to-roll fabrication of flexible thermochromic coatings for smart windows with VO_2 nanoparticles, J. Mater. Chem. C. 6 (2018) 3451–3458. https://doi.org/10.1039/C7TC05876D.

[8] T.D. Vu, Z. Chen, X. Zeng, M. Jiang, S. Liu, Y. Gao, Y. Long, Physical vapour deposition of vanadium dioxide for thermochromic smart window applications, J. Mater. Chem. C. 7 (2019) 2121–2145. https://doi.org/10.1039/C8TC05014G.

[9] D. Mercs, A. Didelot, F. Capon, J.-F. Pierson, B. Hafner, A. Pazidis, S. Föste, R. Reineke-Koch, Innovative Smart Selective Coating to Avoid Overheating in Highly Efficient Thermal Solar Collectors, Energy Procedia. 91 (2016) 84–93. https://doi.org/10.1016/j.egypro.2016.06.177.

[10] A. Paone, M. Geiger, R. Sanjines, A. Schüler, Thermal solar collector with VO_2 absorber coating and $V_{1-x}W_xO_2$ thermochromic glazing – Temperature matching and triggering, Sol. Energy. 110 (2014) 151–159. https://doi.org/10.1016/j.solener.2014.08.033.
[11] M. Benkahoul, M. Chaker, J. Margot, E. Haddad, R. Kruzelecky, B. Wong, W. Jamroz, P. Poinas, Thermochromic VO_2 film deposited on Al with tunable thermal emissivity for space applications, Sol. Energy Mater. Sol. Cells. 95 (2011) 3504–3508. https://doi.org/10.1016/j.solmat.2011.08.014.
[12] A. Hendaoui, N. Émond, S. Dorval, M. Chaker, E. Haddad, Enhancement of the positive emittance-switching performance of thermochromic VO_2 films deposited on Al substrate for an efficient passive thermal control of spacecrafts, Curr. Appl. Phys. 13 (2013) 875–879. https://doi.org/10.1016/j.cap.2012.12.028.
[13] A. Hendaoui, N. Émond, S. Dorval, M. Chaker, E. Haddad, VO_2-based smart coatings with improved emittance-switching properties for an energy-efficient near room-temperature thermal control of spacecrafts, Sol. Energy Mater. Sol. Cells. 117 (2013) 494–498. https://doi.org/10.1016/j.solmat.2013.07.023.
[14] A.L. Pergament, G.B. Stefanovich, A.A. Velichko, Oxide Electronics and Vanadium Dioxide Perspective: A Review, J. Sel. Top. NANO Electron. Comput. 1 (2013) 24–43. https://doi.org/10.15393/j8.art.2013.3002.
[15] D.-H. Qiu, Q.-Y. Wen, Q.-H. Yang, Z. Chen, Y.-L. Jing, H.-W. Zhang, Electrically-driven metal–insulator transition of vanadium dioxide thin films in a metal–oxide-insulator–metal device structure, Mater. Sci. Semicond. Process. 27 (2014) 140–144. https://doi.org/10.1016/j.mssp.2014.06.030.
[16] Y.-B. Kang, Critical evaluation and thermodynamic optimization of the VO–$VO_{2.5}$ system, J. Eur. Ceram. Soc. 32 (2012) 3187–3198. https://doi.org/10.1016/j.jeurceramsoc.2012.04.045.
[17] H. Yuce, H. Alaboz, Y. Demirhan, M. Ozdemir, L. Ozyuzer, G. Aygun, Investigation of electron beam lithography effects on metal–insulator transition behavior of vanadium dioxide, Phys. Scr. 92 (2017) 114007. https://doi.org/10.1088/1402-4896/aa90a3.
[18] Y. Zhao, C. Chen, X. Pan, Y. Zhu, M. Holtz, A. Bernussi, Z. Fan, Tuning the properties of VO_2 thin films through growth temperature for infrared and terahertz modulation applications, J. Appl. Phys. 114 (2013) 113509. https://doi.org/10.1063/1.4821846.
[19] M. Zhu, H. Qi, B. Wang, H. Wang, T. Guan, D. Zhang, Thermochromism of vanadium dioxide films controlled by the thickness of ZnO buffer layer under low substrate temperature, J. Alloys Compd. 740 (2018) 844–851. https://doi.org/10.1016/j.jallcom.2018.01.066.
[20] D. Brassard, S. Fourmaux, M. Jean-Jacques, J.C. Kieffer, M.A. El Khakani, Grain size effect on the semiconductor-metal phase transition characteristics of magnetron-sputtered VO_2 thin films, Appl. Phys. Lett. 87 (2005) 051910. https://doi.org/10.1063/1.2001139.
[21] J.B.K. Kana, J.M. Ndjaka, P.O. Ateba, B.D. Ngom, N. Manyala, O. Nemraoui, A.C. Beye, M. Maaza, Thermochromic VO_2 thin films synthesized by rf-inverted cylindrical magnetron sputtering, Appl. Surf. Sci. 254 (2008) 3959–3963. https://doi.org/10.1016/j.apsusc.2007.12.021.
[22] V. Melnik, I. Khatsevych, V. Kladko, A. Kuchuk, V. Nikirin, B. Romanyuk, Low-temperature method for thermochromic high ordered VO_2 phase formation, Mater. Lett. 68 (2012) 215–217. https://doi.org/10.1016/j.matlet.2011.10.075.
[23] Q. Yu, W. Li, J. Liang, Z. Duan, Z. Hu, J. Liu, H. Chen, J. Chu, Oxygen pressure manipulations on the metal–insulator transition characteristics of highly (0 1 1)-oriented vanadium dioxide films grown by magnetron sputtering, J. Phys. Appl. Phys. 46 (2013) 055310. https://doi.org/10.1088/0022-3727/46/5/055310.
[24] Y.-K. Dou, J.-B. Li, M.-S. Cao, D.-Z. Su, F. Rehman, J.-S. Zhang, H.-B. Jin, Oxidizing annealing effects on VO_2 films with different microstructures, Appl. Surf. Sci. 345 (2015) 232–237. https://doi.org/10.1016/j.apsusc.2015.03.044.
[25] J. Yoon, C. Park, S. Park, B.S. Mun, H. Ju, Correlation between surface morphology and electrical properties of VO_2 films grown by direct thermal oxidation method, Appl. Surf. Sci. 353 (2015) 1082–1086. https://doi.org/10.1016/j.apsusc.2015.07.036.

[26] X. Xu, A. Yin, X. Du, J. Wang, J. Liu, X. He, X. Liu, Y. Huan, A novel sputtering oxidation coupling (SOC) method to fabricate VO_2 thin film, Appl. Surf. Sci. 256 (2010) 2750–2753. https://doi.org/10.1016/j.apsusc.2009.11.022.
[27] F. Kubel, W. Lengauer, K. Yvon, K. Knorr, A. Junod, Structural phase transition at 205 K in stoichiometric vanadium nitride, Phys. Rev. B. 38 (1988) 12908–12912. https://doi.org/10.1103/PhysRevB.38.12908.
[28] A.B. Mei, O. Hellman, N. Wireklint, C.M. Schlepütz, D.G. Sangiovanni, B. Alling, A. Rockett, L. Hultman, I. Petrov, J.E. Greene, Dynamic and structural stability of cubic vanadium nitride, Phys. Rev. B. 91 (2015) 054101. https://doi.org/10.1103/PhysRevB.91.054101.
[29] H. Guo, C. Lu, Z. Zhang, B. Liang, J. Jia, Comparison of microstructures and properties of VN and VN/Ag nanocomposite films fabricated by pulsed laser deposition, Appl. Phys. A. 124 (2018) 694. https://doi.org/10.1007/s00339-018-2055-x.
[30] N. Fateh, G.A. Fontalvo, G. Gassner, C. Mitterer, The Beneficial Effect of High-Temperature Oxidation on the Tribological Behaviour of V and VN Coatings, Tribol. Lett. 28 (2007) 1–7. https://doi.org/10.1007/s11249-007-9241-x.
[31] G. Rampelberg, B.D. Schutter, W. Devulder, K. Martens, I. Radu, C. Detavernier, In situ X-ray diffraction study of the controlled oxidation and reduction in the V–O system for the synthesis of VO_2 and V_2O_3 thin films, J. Mater. Chem. C. 3 (2015) 11357–11365. https://doi.org/10.1039/C5TC02553B.
[32] C. Zhang, Q. Yang, C. Koughia, F. Ye, M. Sanayei, S.-J. Wen, S. Kasap, Characterization of vanadium oxide thin films with different stoichiometry using Raman spectroscopy, Thin Solid Films. 620 (2016) 64–69. https://doi.org/10.1016/j.tsf.2016.07.082.
[33] F. Ureña-Begara, A. Crunteanu, J.-P. Raskin, Raman and XPS characterization of vanadium oxide thin films with temperature, Appl. Surf. Sci. 403 (2017) 717–727. https://doi.org/10.1016/j.apsusc.2017.01.160.
[34] J.C. Parker, Raman scattering from VO_2 single crystals: A study of the effects of surface oxidation, Phys. Rev. B. 42 (1990) 3164–3166. https://doi.org/10.1103/PhysRevB.42.3164.
[35] P. Schilbe, Raman scattering in VO_2, Phys. B Condens. Matter. 316–317 (2002) 600–602. https://doi.org/10.1016/S0921-4526(02)00584-7.
[36] R. Baddour-Hadjean, J.P. Pereira-Ramos, C. Navone, M. Smirnov, Raman Microspectrometry Study of Electrochemical Lithium Intercalation into Sputtered Crystalline V_2O_5 Thin Films, Chem. Mater. 20 (2008) 1916–1923. https://doi.org/10.1021/cm702979k.
[37] X. Xu, X. He, G. Wang, X. Yuan, X. Liu, H. Huang, S. Yao, H. Xing, X. Chen, J. Chu, The study of optimal oxidation time and different temperatures for high quality VO_2 thin film based on the sputtering oxidation coupling method, Appl. Surf. Sci. 257 (2011) 8824–8827. https://doi.org/10.1016/j.apsusc.2011.04.068.
[38] N.R. Mlyuka, G.A. Niklasson, C.G. Granqvist, Thermochromic VO_2-based multilayer films with enhanced luminous transmittance and solar modulation, Phys. Status Solidi A. 206 (2009) 2155–2160. https://doi.org/10.1002/pssa.200881798.
[39] R.L. Voti, M.C. Larciprete, G. Leahu, C. Sibilia, M. Bertolotti, Optimization of thermochromic VO_2 based structures with tunable thermal emissivity, J. Appl. Phys. 112 (2012) 034305. https://doi.org/10.1063/1.4739489.
[40] P. Jin, G. Xu, M. Tazawa, K. Yoshimura, Design, formation and characterization of a novel multifunctional window with VO_2 and TiO_2 coatings, Appl. Phys. A. 77 (2003) 455–459. https://doi.org/10.1007/s00339-002-1460-2.
[41] J. Zheng, S. Bao, P. Jin, TiO_2(R)/ VO_2 (M)/TiO_2(A) multilayer film as smart window: Combination of energy-saving, antifogging and self-cleaning functions, Nano Energy. 11 (2015) 136–145. https://doi.org/10.1016/j.nanoen.2014.09.023.

[42] J.-H. Yu, S.-H. Nam, J.W. Lee, J.-H. Boo, Enhanced Visible Transmittance of Thermochromic VO_2 Thin Films by SiO_2 Passivation Layer and Their Optical Characterization, Materials. 9 (2016) 556. https://doi.org/10.3390/ma9070556.

[43] L. Kang, Y. Gao, H. Luo, J. Wang, B. Zhu, Z. Zhang, J. Du, M. Kanehira, Y. Zhang, Thermochromic properties and low emissivity of ZnO:Al/VO_2 double-layered films with a lowered phase transition temperature, Sol. Energy Mater. Sol. Cells. 95 (2011) 3189–3194. https://doi.org/10.1016/j.solmat.2011.06.047.

[44] S. Long, X. Cao, N. Li, Y. Xin, G. Sun, T. Chang, S. Bao, P. Jin, Application-oriented VO_2 thermochromic coatings with composite structures: Optimized optical performance and robust fatigue properties, Sol. Energy Mater. Sol. Cells. 189 (2019) 138–148. https://doi.org/10.1016/j.solmat.2018.09.023.

Figure Captions

Figure 1: X-ray diffractograms of as-deposited VN film on silicon substrate and the resulting oxide films after air-oxidation at 450°C for various durations.

Figure 2: Raman spectra of air-oxidized VN films at 450°C for various durations.

Figure 3: Top-view SEM images corresponding to a) the as-deposited VN films and sample oxidized during 10, 20, 25, 30 and 50 minutes for b), c), d), e) and f) respectively.

Figure 4: a) TEM cross-sectional image of sample VN_25. b) HRTEM image of the highlighted red area in Fig. 4 a). c) FFT from the region of Fig. 4 b).

Figure 5: a) High angle annular dark field image of the sample VN_25, EELS characterization was performed in the four zones (labeled from 1 to 4). b) EELS spectra of the four different zones of Fig. 5a). The color of each curve corresponds to the area of the same color where the spectrum was conducted.

Figure 6: Thermal camera measurements of apparent infrared temperatures (T_{IR}), as a function of sample temperature (T_S) for VN films oxidized between 15 and 35 minutes. Measurements are carried out by considering $\varepsilon = 1$ irrespective to the sample. Up and down triangles represent the profiles for temperature ramping up and down, respectively. The infrared camera works on the range of 7.5-13 µm. The red lines obtained by a linear fitting in the low temperature (LT) and high temperature region (HT) enabled the determination of emissivity values before and after MIT.

Figure 7: Sheet resistance (SR) as a function of the temperature for all oxidized VN films deposited on silicon substrate.

Figure 8: Logarithm of the ratio of sheet resistance at low and high temperature (left axis, blue squares), emissivity switch (right axis, red circles) as a function of oxidation time. We used a color gradient to illustrate the different five regions for the structure of oxidized films at 450 °C.

Figure 1

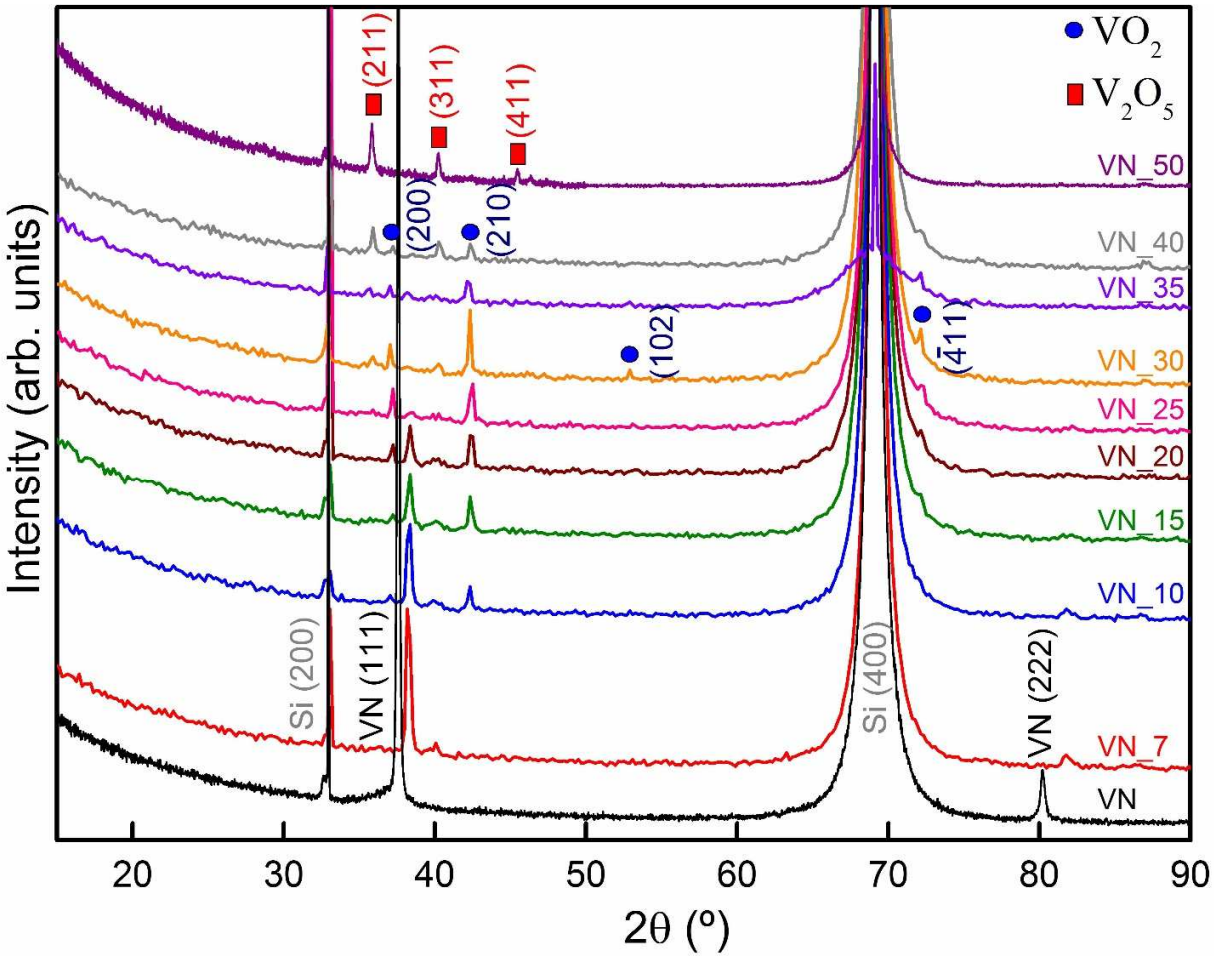
VO2
V2O5
(211)
(311)
(411)
(200)
(210)
(102)
(4̄11)
VN_50
VN_40
VN_35
VN_30
VN_25
VN_20
VN_15
VN_10
VN_7
VN
Si (200)
VN (111)
Si (400)
VN (222)
Intensity (arb. units)
20
30
40
50
60
70
80
90
2θ (°)

Figure 2

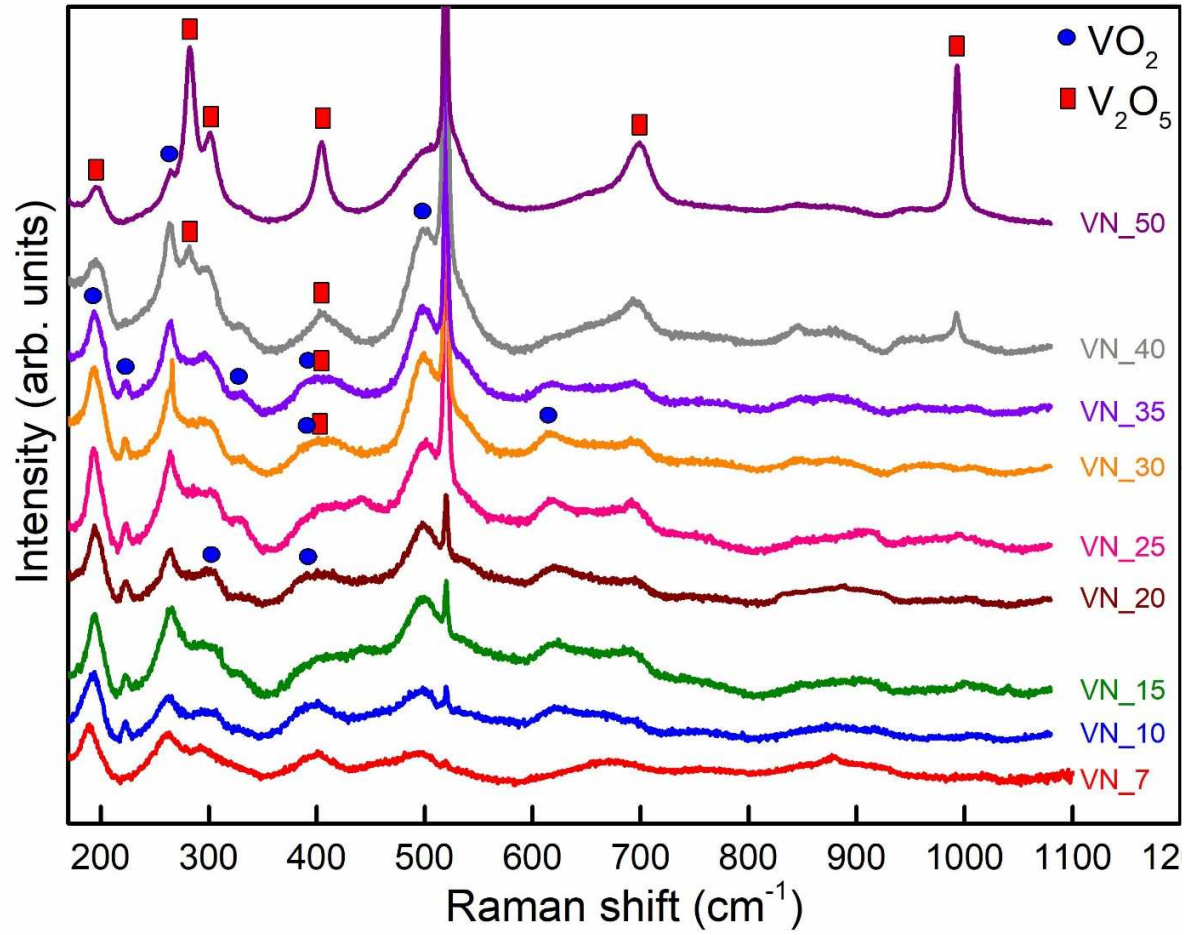
VO2
V2O5
VN_50
VN_40
VN_35
VN_30
VN_25
VN_20
VN_15
VN_10
VN_7
Intensity (arb. units)
200
300
400
500
600
700
800
900
1000
1100
12
Raman shift (cm-1)

Figure 3

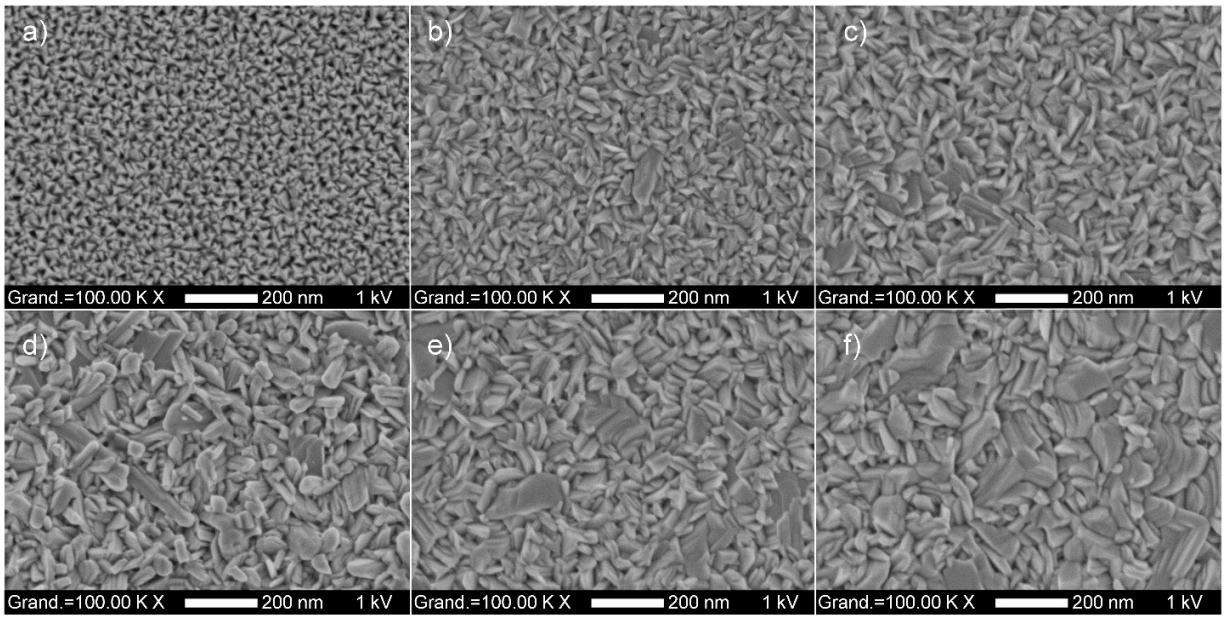
a)
Grand.=100.00 K X 200 nm 1 kV
b)
Grand.=100.00 K X 200 nm 1 kV
c)
Grand.=100.00 K X 200 nm 1 kV
d)
Grand.=100.00 K X 200 nm 1 kV
e)
Grand.=100.00 K X 200 nm 1 kV
f)
Grand.=100.00 K X 200 nm 1 kV

Figure 4

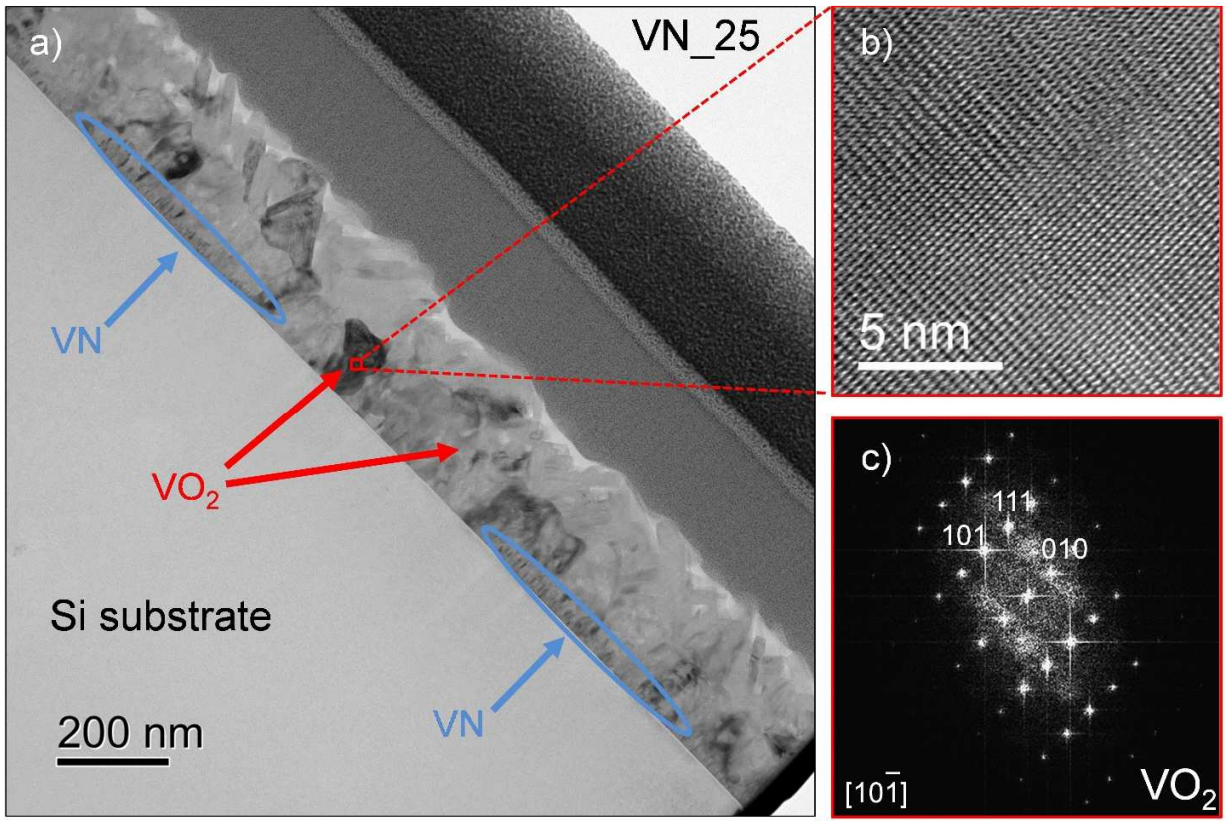
a)
VN_25
VN
VO_2
Si substrate
200 nm
VN
b)
5 nm
c)
111
101
010
[10$\bar{1}$]
VO_2

Figure 5

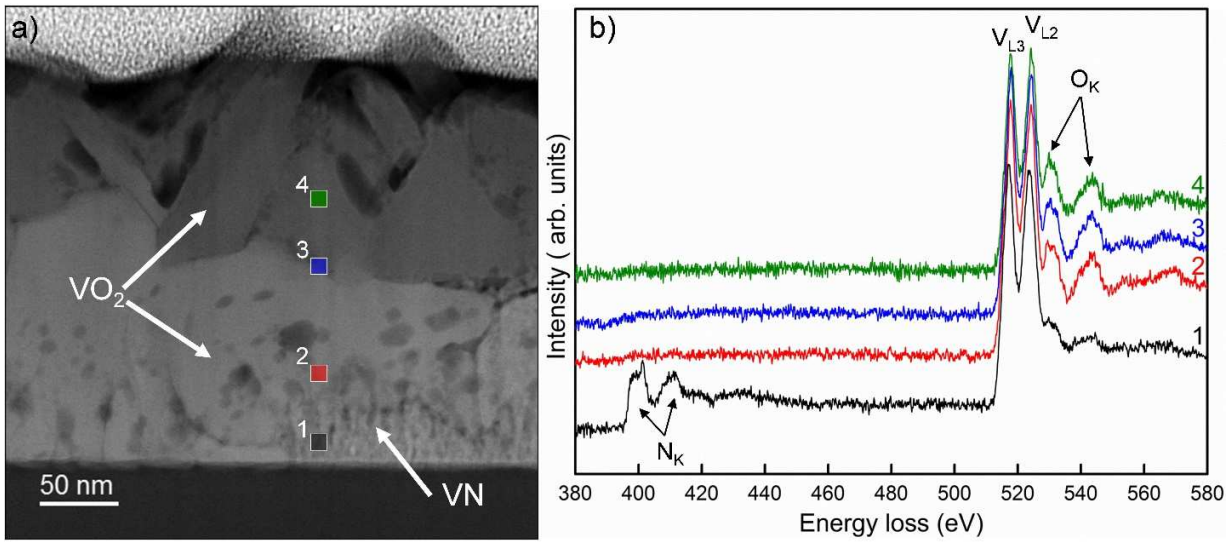
a)
4
3
2
1
VO2
50 nm
VN
b)
VL3
VL2
OK
NK
4
3
2
1
Intensity (arb. units)
380
400
420
440
460
480
500
520
540
560
580
Energy loss (eV)

Figure 6:

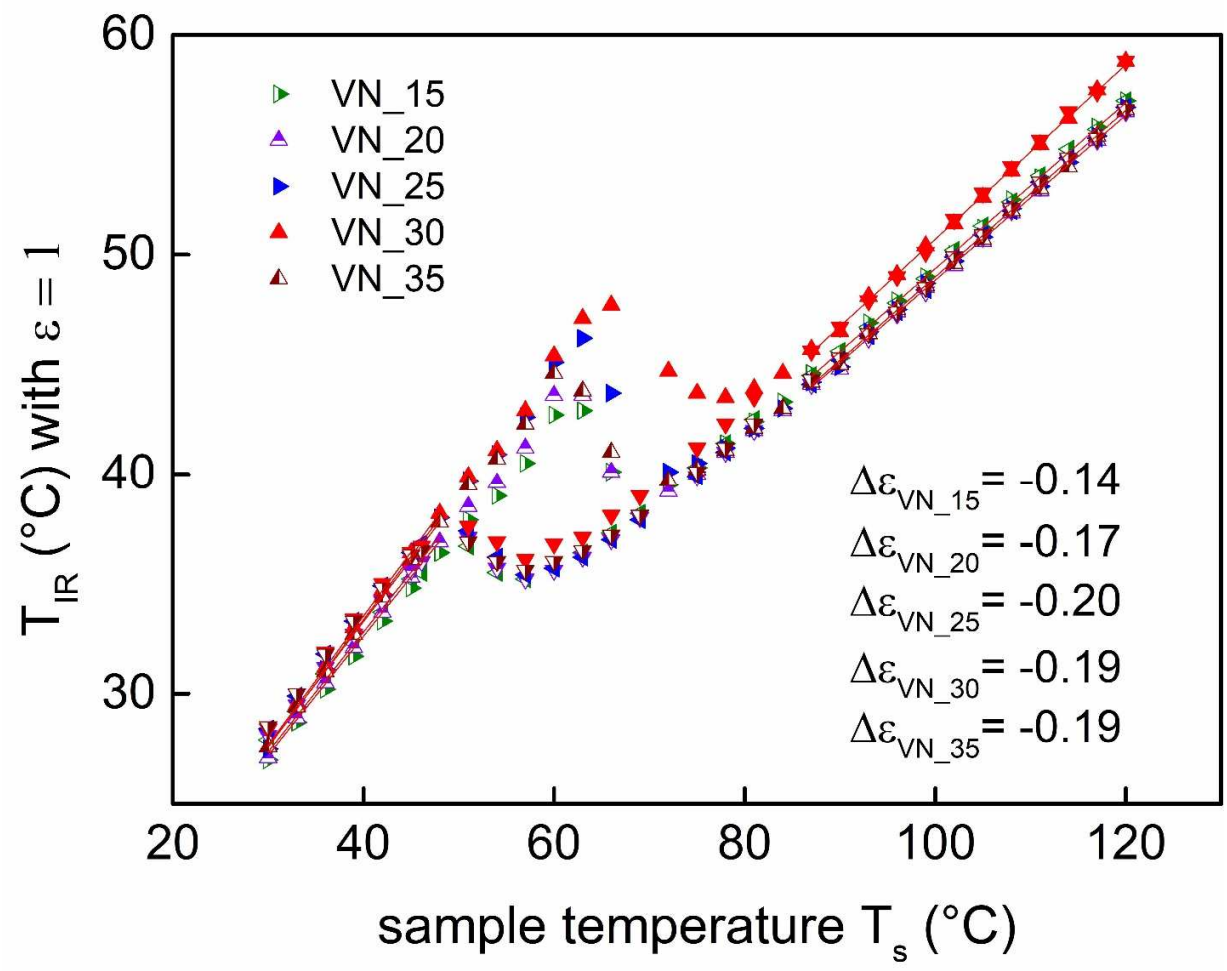
VN_15
VN_20
VN_25
VN_30
VN_35
$\Delta\varepsilon_{VN\_15}$= -0.14
$\Delta\varepsilon_{VN\_20}$= -0.17
$\Delta\varepsilon_{VN\_25}$= -0.20
$\Delta\varepsilon_{VN\_30}$= -0.19
$\Delta\varepsilon_{VN\_35}$= -0.19
T_{IR} (°C) with ε = 1
sample temperature T_s (°C)
60
50
40
30
20
40
60
80
100
120

Figure 7:

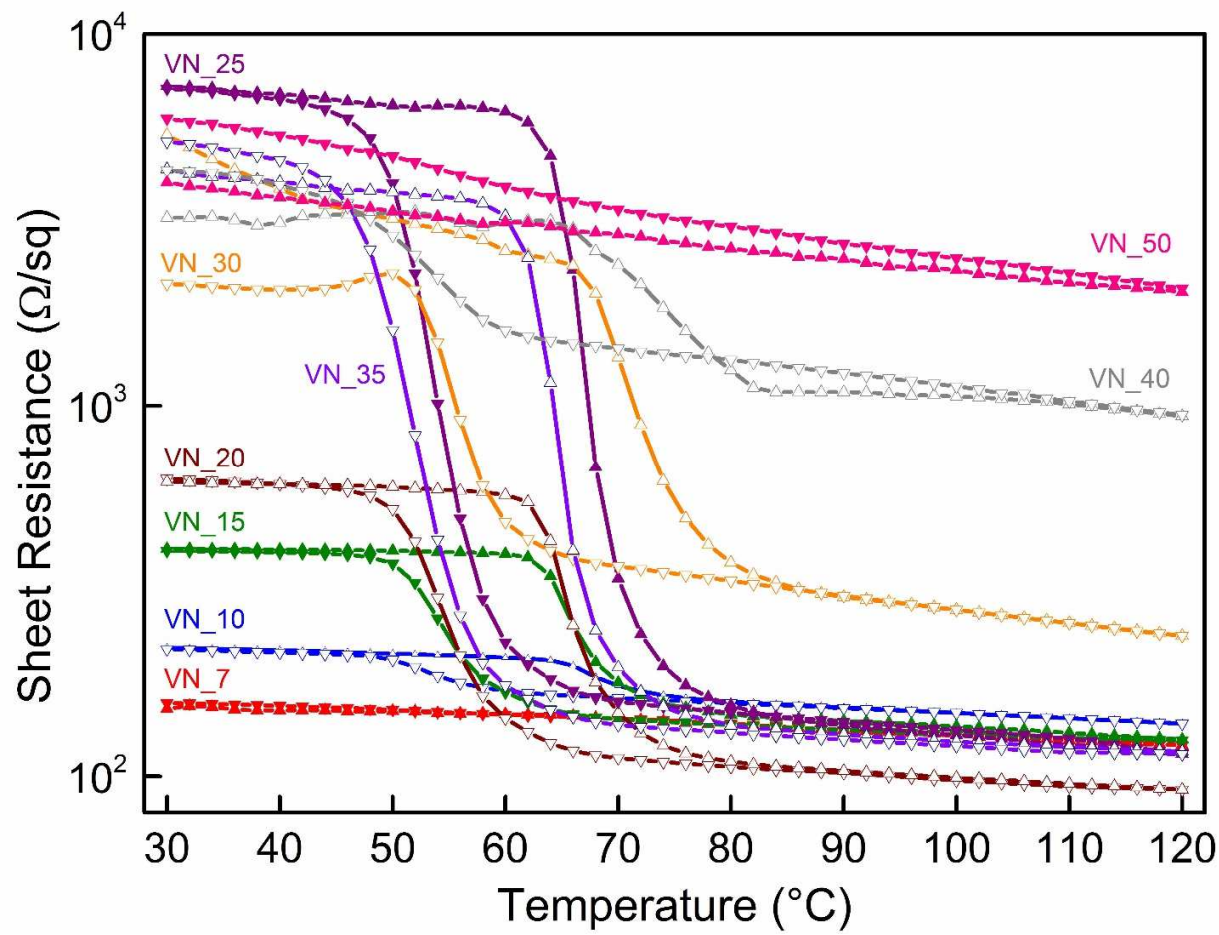
Sheet Resistance (Ω/sq)
Temperature (°C)
VN_25
VN_50
VN_30
VN_35
VN_40
VN_20
VN_15
VN_10
VN_7

Figure 8:

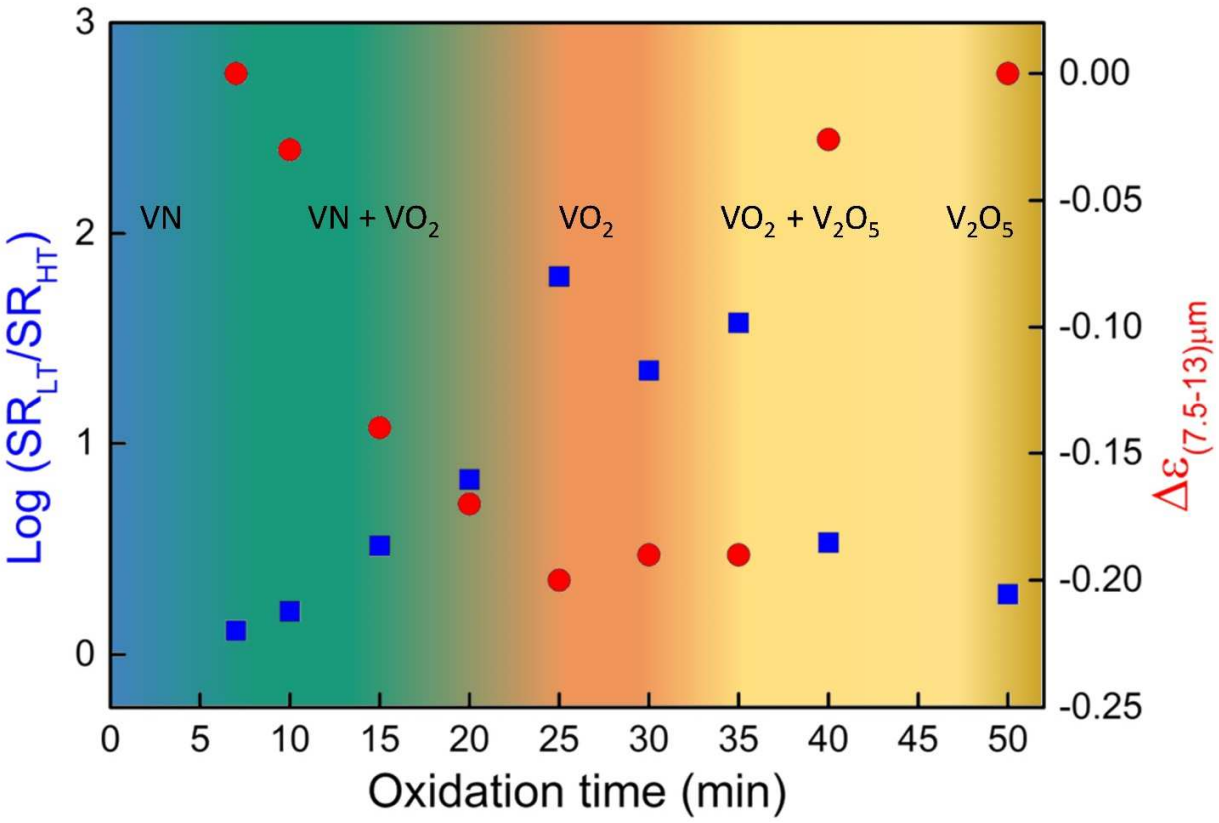
VN
VN + VO2
VO2
VO2 + V2O5
V2O5
Log (SRLT/SRHT)
Δε(7.5-13)μm
Oxidation time (min)
0
1
2
3
0.00
-0.05
-0.10
-0.15
-0.20
-0.25
0
5
10
15
20
25
30
35
40
45
50